Journal of Catalysis **184,** 535–549 (1999)
Article ID jcat.1999.2464, available online at http://www.idealibrary.com on IDEAL®

Transition Metal Bimetallic Oxycarbides: Synthesis, Characterization, and Activity Studies

S. Ted Oyama,[1] C. Charles Yu, and S. Ramanathan

Environmental Catalysis and Materials Laboratory, Department of Chemical Engineering, Virginia Tech., Blacksburg, Virginia 24061-0211

Received December 2, 1998; revised February 23, 1999; accepted February 26, 1999

A new family of bimetallic oxycarbide compounds M^{I}–M^{II}–O–C (M^{I} = Mo, W; M^{II} = V, Nb, Cr, Fe, Co, Ni) has been synthesized by carburizing bimetallic oxide precursors using a temperature-programmed method. The oxide precursors are prepared by conventional solid-state reaction between two appropriate monometallic oxides. The synthesis involves passing a 20 mol% CH_4 in H_2 mixture over the oxide precursors while raising the temperature at a linear rate of 8.3×10^{-2} K s^{-1} (5 K/min) to a final temperature (T_{max}) which is held for a period of time (t_{hold}). The synthesis, chemisorption properties, and reactivation of the materials indicate that the compounds can be divided into two groups of different reducibility (high and low). Their surface activity and surface area are evaluated based on CO chemisorption and N_2 physisorption measurements. It is found that the CO number density correlates with the reducibility of the compounds.

The catalysts were evaluated for hydroprocessing in a three-phase trickle-bed reactor operated at 3.1 MPa and 643 K. The feed was a model liquid mixture containing 3000 ppm sulfur (dibenzothiophene), 2000 ppm nitrogen (quinoline), 500 ppm oxygen (benzofuran), 20 wt% aromatics (tetralin), and balance aliphatics (tetradecane). The bimetallic oxycarbides had moderate activity for HDN of quinoline, with Nb–Mo–O–C showing higher HDN than a commercial sulfided Ni–Mo/Al_2O_3 catalyst tested at the same conditions. X-ray diffraction of the spent catalysts indicated that the oxycarbides of the early transition metals were tolerant of sulfur, while those involving the late transition metals showed bulk sulfide phases.

INTRODUCTION

As world reserves of petroleum diminish, the quality of feedstocks will tend to decrease as available crudes are increasingly contaminated with nitrogen, sulfur, and metals. Removal of these substances from the hydrocarbon resource will grow in importance. Traditional catalysts that carry out this upgrading are supported sulfides like Ni–Mo–S/Al_2O_3 or Co–Mo–S/Al_2O_3. We were the first to report the preparation and reactivity of bimetallic oxynitrides (1, 2, 3). This paper concerns the preparation of a new class of hydroprocessing catalysts composed of transition metal bimetallic oxycarbides. The compounds are formed by alloying Mo and W with other transition metals (V, Nb, Cr, Fe, Co, and Ni). A preliminary report of the Mo–Nb system has been published (4). Because nitrogen removal is more difficult than sulfur removal, the focus of the catalytic studies will be on hydrodenitrogenation.

In recent years, transition metal carbides have received considerable attention as catalysts (5–11). Molybdenum and tungsten carbides are particular attractive because they resemble the noble group 8–10 metals (Pt, Pd, Rh, etc.) in catalytic activity and in some cases offer superior selectivity, stability, and resistance to poisoning (12–15). Considerable work has been done on the application of these compounds to hydroprocessing (16–19). Recently, a number of studies on bimetallic nitrides have appeared (20–22).

Most *monometallic* transition metal carbides are composed of close-packed or near-close-packed metal arrays with the carbon atoms occupying the interstitial sites between metal atoms. For this reason, these carbides are sometimes termed interstitial alloys. Each carbon is surrounded by six metal atoms located at the corners of octahedra or trigonal prisms. The different atomic packings adopted by carbides and nitrides is described by Hägg's rule (23). Basically, simple structures are formed if the radius ratio of nonmetal to metal (r value) is less than 0.59. The effect of electron count on crystal structure has also been described (24).

Complete filling of all the octahedral sites in a cubic close-packed (ABC, ABC, . . . sequence) metal array with carbon results in the $B1$ (NaCl) structure common for monocarbides, e.g., TiC, ZrC, HfC, VC, NbC, TaC, etc. Random filling of half of the octahedral sites in the hexagonal close-packed metal array (AB, AB, . . . sequence) results in the L'_3 structure common among the subcarbides, e.g., V_2C, Nb_2C, Ta_2C, Mo_2C, W_2C. Orderly filling half of the trigonal-prism sites (all the B sites) in the simple hexagonal metal array (A, A, . . . sequence) results in the WC structure, e.g., WC. The structures described above are examples of the simplest forms adopted by most of the binary metal carbides.

[1] To whom correspondence should be addressed.

0021-9517/99 $30.00

Deviations occur when the r value exceeds 0.59. For example, Cr_3C_2, with an r value of 0.61, is orthorhombic.

In contrast to the monometallic compounds, bimetallic carbides generally have complex structures, and a number have been reported in the literature. The β-Mn type carbides have general formula $M^{I}_{x}M^{II}_{y}C_z$ ($x=3$, $y=2$, $z=1$) with M^{I} usually a transition metal and M^{II} a group 11–13 element (25). The crystal structure of these compounds is cubic (space group $P4_132$) (26). The perovskite-type carbides have general formula $M^{I}_{x}M^{II}_{y}C_z$ ($x=3$, $y=1$, $z=0.3$–1.2) with M^{I} usually a transition metal and M^{II} a group 12–14 element (27). The crystal structure of these compounds is cubic (space group $Fm3m$). The H-type carbides have general formula $M^{I}_{x}M^{II}_{y}C_z$ ($x=2$, $y=1$, $z=1$) also with M^{I} a transition metal and M^{II} a group 12–14 element. The crystal structure of these compounds is hexagonal (space group $P6_3/mmc$) (28). The κ-type carbides have a general formula $M^{I}_{x}M^{II}_{y}C_z$ ($x=9$, $y=3$, $z=4$) with a hexagonal crystal structure (space group $P6_3/mmc$) (29). The η_1-type carbides have general formula $M^{I}_{3}M^{II}_{3}C_x$ ($x=0.5$–1) (30) and the η_2-type carbides have general formula $M^{I}_{2}M^{II}_{4}C$. Both of them have cubic crystal structures (space group $Fd3m$) (31). The κ- and η-carbides are generally formed between an early and a late transition metal.

In this paper we report a new class of oxycarbides with a general formula $M^{I}_{x}M^{II}_{y}C_zO_w$ ($x=1$–2, $y=1$–2, $z=1$–5 and $w=0$–3) with $M^{I}=$ Mo or W and $M^{II}=$ V, Cr, Mn, Nb, Fe, Co, and Ni (Groups 5–10). These compounds can be distinguished from previously reported compounds from their composition and crystal structure. Whereas other bimetallic carbides generally have low molar concentrations of carbon, these compounds have high proportions of the nonmetallic component (C and O). Also previously reported compounds have complex structures, whereas the compounds in the present work have mostly simple cubic or hexagonal structures.

EXPERIMENTAL

A. Materials

Materials used in the current investigation were molybdenum (VI) oxide (MoO_3, 99.95%, Johnson Matthey), tungsten (VI) oxide (WO_3, 99.8%, Johnson Matthey), vanadium (V) oxide (V_2O_5, 99.9%, Johnson Matthey), niobium (V) oxide (Nb_2O_5, 99.9%, Johnson Matthey), nickel (II) oxide (NiO, 99%, Johnson Matthey), chromium (III) oxide (Cr_2O_3, 98%, Aldrich), manganese (II, III) oxide (Mn_3O_4, Mn 71%, Johnson Matthey), iron (III) oxide (Fe_2O_3, 99.9%, Johnson Matthey), and cobalt (II, III) oxide (Co_3O_4, Co 72%, Aldrich). The gases employed were 20% CH_4/H_2 (Airco, UHP Grade), He (Airco, Grade 5.0), and 0.5% O_2/He (Airco, UHP Grade).

TABLE 1

Preparation Conditions for Bimetallic Oxides

System (M_{II}–M_I)	Starting materials	Metal ratio ($M_{II}:M_I$)	Firing temp. (T_{MAX})	Time hold at T_{MAX}
V–Mo–O	V_2O_5–MoO_3	2:1	948 K	6 h
Nb–Mo–O	Nb_2O_5–MoO_3	2:3	1058 K	6 h
Cr–Mo–O	Cr_2O_3–MoO_3	1:1	1058 K	6 h
Fe–Mo–O	Fe_2O_3–MoO_3	1:1	1058 K	6 h
Ni–Mo–O	NiO–MoO_3	1:1	1058 K	6 h
V–W–O	V_2O_5–WO_3	1:1	1323 K	6 h
Nb–W–O	Nb_2O_5–WO_3	2:3	1323 K	6 h
Mo–W–O	MoO_3–WO_3	1:1	1058 K	6 h
Fe–W–O	Fe_2O_3–MoO_3	2:1	1323 K	10 h
Co–W–O	Co_3O_4–WO_3	1:1	1373 K	6 h
Ni–W–O	NiO–W_3	1:1	1323 K	10 h

B. Synthesis of Catalysts

Bimetallic oxide precursors were prepared by the solid state fusion of two monometallic oxides. In all cases one of the oxides was MoO_3 or WO_3. The two monometallic oxides, at a prechosen metal ratio (Table 1), were first ground together using a mortar and pestle with added ethanol to achieve better dispersion. They were then partially dried and pressed at about 55 MPa (8000 psi) in a 1.25 cm (1/2 inch) diameter hard steel die. Since the remaining ethanol in the mixture facilitated compacting, no chemical binder was needed for pressing. The oxide compacts ($\sim$1 g, each) were subsequently fired at high temperature for 6 h and were finally cooled to room temperature and pulverized to a micrometer-sized powder in preparation for the carbiding step. The preparation conditions for the bimetallic oxides, including starting materials used, metal ratios chosen, and final firing temperatures, are summarized in Table 1.

Bimetallic oxycarbides were prepared by the temperature programmed synthesis (TPS) of the bimetallic oxides with a 20% CH_4/H_2 gas mixture. The bimetallic oxide powders prepared, as described above, were transferred to a quartz reactor, which was placed inside a tubular resistance furnace (Hoskins, 550 W) controlled by a temperature programmer (Omega Model CN2000). A 20% CH_4/H_2 gas mixture was passed through the oxide powders at a flow rate of 2.73×10^{-2} μmol s^{-1} (400 cm^3/min) for a 0.5 $\sim$ 1 g batch and 10.93×10^{-2} μmol s^{-1} (1600 cm^3/min) for a 4 g batch. The temperature was increased at a linear rate of 8.3×10^{-2} K s^{-1} (5 K/min) to a final temperature (T_{max}) which was held for a period of time (t_{hold}). During the TPS process, the effluent gas stream was sampled into a mass spectrometer (Ametek/Dycor Model MA100) chamber through a variable leak valve (Granville Phillips Model 203). A computer (Thoroughbred, 80386SX-16) recorded the mass signals of the effluent gas and the sample temperatures through a

TABLE 2

Synthesis Conditions for Bimetallic Oxycarbides

System (M_{II}–M_I–O–C)	Metal ratio (M_{II} : M_I)	Final temp. (T_{max})	Time hold at T_{max} (t_{hold})
V–Mo–O–C	2 : 1	1053 K	70 min
Nb–Mo–O–C	2 : 3	1063 K	90 min
Cr–Mo–O–C	1 : 1	1073 K	60 min
Fe–Mo–O–C	1 : 1	943 K	35 min
Ni–Mo–O–C	1 : 1	923 K	40 min
V–W–O–C	1 : 1	1153 K	25 min
Nb–W–O–C	2 : 3	1053 K	50 min
Mo–W–O–C	1 : 1	1003 K	30 min
Fe–W–O–C	2 : 1	1033 K	35 min
Co–W–O–C	1 : 1	1053 K	24 min
Ni–W–O–C	1 : 1	973 K	50 min

RS232 interface. At the end of the synthesis the furnace was removed to quench the samples and the flow of 20% CH_4/H_2 mixture gas was switched to helium and maintained during the cooling process (900 s). After cooling, the pure He gas was switched to a gas mixture containing 0.5% O_2 in He. The time of passivation was determined to be sufficient by monitoring the oxygen signal with a mass spectrometer (Ametek/Dycor Model MA100) until it reached steady state. The synthesis conditions of bimetallic oxycarbides, T_{max} and t_{hold}, are listed in Table 2.

C. Characterization

X-ray diffraction (XRD) analysis of both bimetallic oxides and bimetallic oxycarbides was carried out using a powder diffractometer (Scintag, Model XDS2000) with a Cu$K\alpha$ monochromatized radiation source), operated at 40 kV and 25 mA. Elemental analysis of the sample was carried out by atomic absorption spectroscopy. The sample was also characterized by TPR to 728 K, CO chemisorption, and N_2 physisorption. CO up-takes of both *in situ* and passivated/reduced samples were measured.

TPR of the passivated samples was carried out by passing a 10% H_2 in He gas mixture through the samples, placed in quartz microreactors, at a rate of 20.4 μmol s^{-1} (50 cm^3/min). The temperature was increased at a linear rate of 0.16 K s^{-1} (10 K/min) to 728 K, where it was held for 2 h. The temperature of the sample was measured through a chromel–alumel thermocouple placed in a well, located at the center of the reactor bed. As with the TPS the effluent from the reactor was sampled into a mass spectrometer to monitor species desorbed during the heating. At the end of the TPR process, the H_2/He gas mixture was switched to pure He, and the samples were brought to room temperature for CO chemisorption measurements.

CO chemisorption was used to titrate the surface metal atoms in the sample. The *in situ* CO uptake was measured right after the synthesis without exposing the samples to oxygen. Pulses of CO gas were introduced through a sampling valve with the He carrier gas stream passing over the samples. The total uptake was calculated by referring the areas under the CO mass signal (28) peaks to the known quantity of 12.02 μmol CO for a single peak. CO uptake of the reduced sample was measured, in the same way, after a 2 h reduction (described above) of the passivated sample.

Surface area was determined immediately after the CO uptake measurement by a similar flow technique using a 30% N_2 in He gas mixture passed over the sample maintained at liquid nitrogen temperature. The amount of physisorbed N_2 was obtained by comparing the area of the desorption peaks to the area of calibrated N_2 pulses containing 37.95 μmol N_2/pulse. The surface area was then calculated from the single point BET equation.

D. Catalytic Testing

Catalysts were tested in a three-phase trickle-bed reactor (32) operated at 3.1 MPa and 643 K. The testing unit consisted of three parallel reactors immersed in a fluidized sand bath (Techne, Model SBL-2). The temperature of the sand bath was controlled by a temperature controller (Omega, Model 6051K). The reactors were 19 mm/16 mm OD/ID 316 SS tubes with a central thermocouple which measured the temperature of the catalyst bed. The catalysts were in the form of coarse powders and were supported between quartz wool plugs in a 13 mm ID 316 stainless steel basket. Purified hydrogen was compressed to 10.2 MPa and the flow to the reactors was regulated by mass flow controllers (Brooks, Model 5850E). A liquid feed mixture was metered from burettes using high pressure liquid pumps (LDC Analytical, Model NCI 11D5). Liquid samples were collected downstream and analyzed off-line using a gas chromatograph equipped with flame ionization detector.

Experimental runs consisted of testing out a series of transition metal bimetallic carbides for their activity in hydrogenation (HYD), hydrodenitrogenation (HDN), hydrodesulfurization (HDS), and hydrodeoxygenation (HDO) using model compounds at 643 K and 3.1 MPa. A commercial Ni–Mo–S/Al_2O_3 sample (Shell 324) was used as a reference. HYD refers to hydrogenation of aromatic rings without removal of heteroatoms, whereas HDN, HDS, and HDO refer to the total removal of N, S, and O, respectively. The liquid feed mixture consisted of 3000 ppm sulfur (dibenzothiophene, DBT), 2000 ppm nitrogen (quinoline, QNL), 500 ppm oxygen (benzofuran, BZF), 20 wt% aromatics (tetralin, TTL), and balance aliphatics (tetradecane, TTD). A typical experiment consisted of loading about 0.2–5.3 g (powder of particle size ca. 1 μm) of the catalyst equivalent to a total surface area of 30 m^2. The catalysts were physically mixed with quartz chips (35/45 mesh), if required, to make up a bed volume of 1 cm^3. Prior to catalytic testing, the bimetallic carbides were activated in flowing hydrogen while the Ni–Mo/Al_2O_3 catalyst was sulfided using

a 10% H_2S/H_2 gas mixture as described by the manufacturer. The pretreatment was carried out *in situ* at 723 K and atmospheric pressure for 3 h. After the pretreatment, the reactors were cooled down to the reaction temperature (643 K) and hydrogen was pressurized to 3.1 MPa. The liquid feed rate was adjusted to 5 cm^3/h and the hydrogen flow rate was set at 150 cm^3(NTP)/min (100 μmol s^{-1}). Samples were collected at regular intervals for a period of 60 h by which time the catalysts showed steady state activity. Blank experiments with quartz chips duly indicated negligible activity of the empty reactors.

After the reaction, the spent catalysts were cleaned with hexane solvent for 24 h to wash out any residual liquid on the catalyst surface and air dried until the solvent evaporated. The bulk composition of the catalysts was identified by X-ray diffraction.

RESULTS

Figures 1a–1k show the XRD patterns of oxides after solid state reaction. For comparison, the XRD patterns of the starting monoxides are shown in Figs. 2a–2h. The prominent features of each product's XRD pattern, i.e., peak position and intensity, do not match those of the parent oxides, nor their reduced forms. The results suggest that at least the major phases of the products are true bimetallic oxides, instead of mechanical mixtures of the starting oxides.

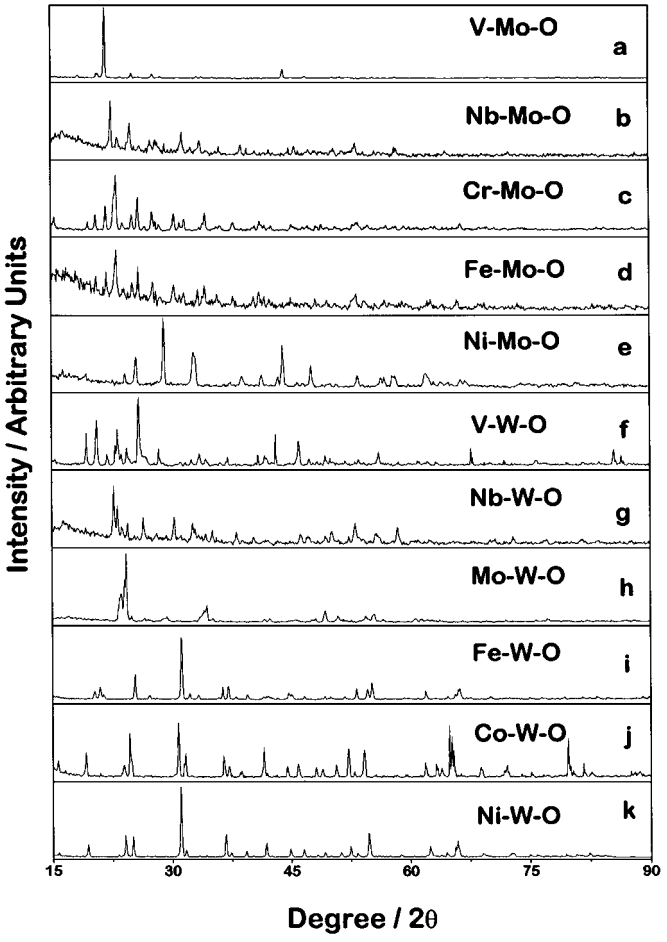

FIG. 1. X-ray diffraction patterns of bimetallic oxides.

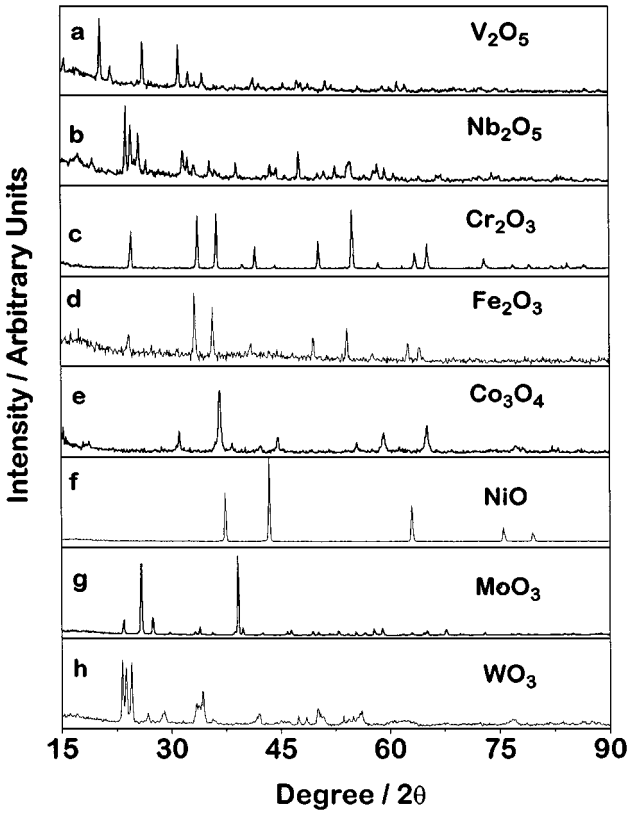

FIG. 2. X-ray diffraction patterns of parent monometallic oxides.

Figures 3a–3k show the synthesis traces of masses (M) 2, 15, 18, 28, and 44, as well as the temperature profile during the reaction. The signals at $M = 2$ and 15 represent hydrogen and methane, while the signals at $M = 18$, 28, and 44 represent water, carbon monoxide, and carbon dioxide, respectively. The XRD patterns of the oxycarbides synthesized are shown in Figs. 4a–4k.

Table 3 reports the elemental composition of the bimetallic oxycarbides. Comparison is made to the nominal "theoretical" metal mole ratio based on the preparation stoichiometry.

Table 4 lists the calculated CO uptakes, surface areas, and the active site densities of the *in situ* and passivated oxycarbides. The surface area of the samples varies from low (5 $m^2 g^{-1}$) to high (124 $m^2 g^{-1}$). The CO uptake ranges from zero to moderate (186 μmol g^{-1}) for the reduced samples, and it ranges from zero to high (520 μmol g^{-1}) for the *in situ* samples.

TABLE 3

Molar Composition of Bimetallic Oxycarbide M^{I}–M^{II}–O–C (from Elemental Analysis)

Sample	$M^{II}:M^{I}$ (Theoretical)	M^{II}						M^{I}			
		V	Nb	Cr	Fe	Co	Ni	Mo	W	C	O
V–Mo–O–C	2:1	2.0						0.9		1.9	1.5
Nb–Mo–O–C	2:3		2.0					2.4		4.7	2.6
Cr–Mo–O–C	1:1										
Fe–Mo–O–C	1:1				1.0			1.0		0.49	0.58
Ni–Mo–O–C	1:1						1.0	0.9		0.46	0.14
V–W–O–C	1:1	1.0							0.9	2.1	—
Nb–W–O–C	2:3		1.0						1.0	1.3	—
Mo–W–O–C	1:1							1.0	1.0	1.0	1.9
Ni–W–O–C	1:1					1.0			1.0	1.0	—

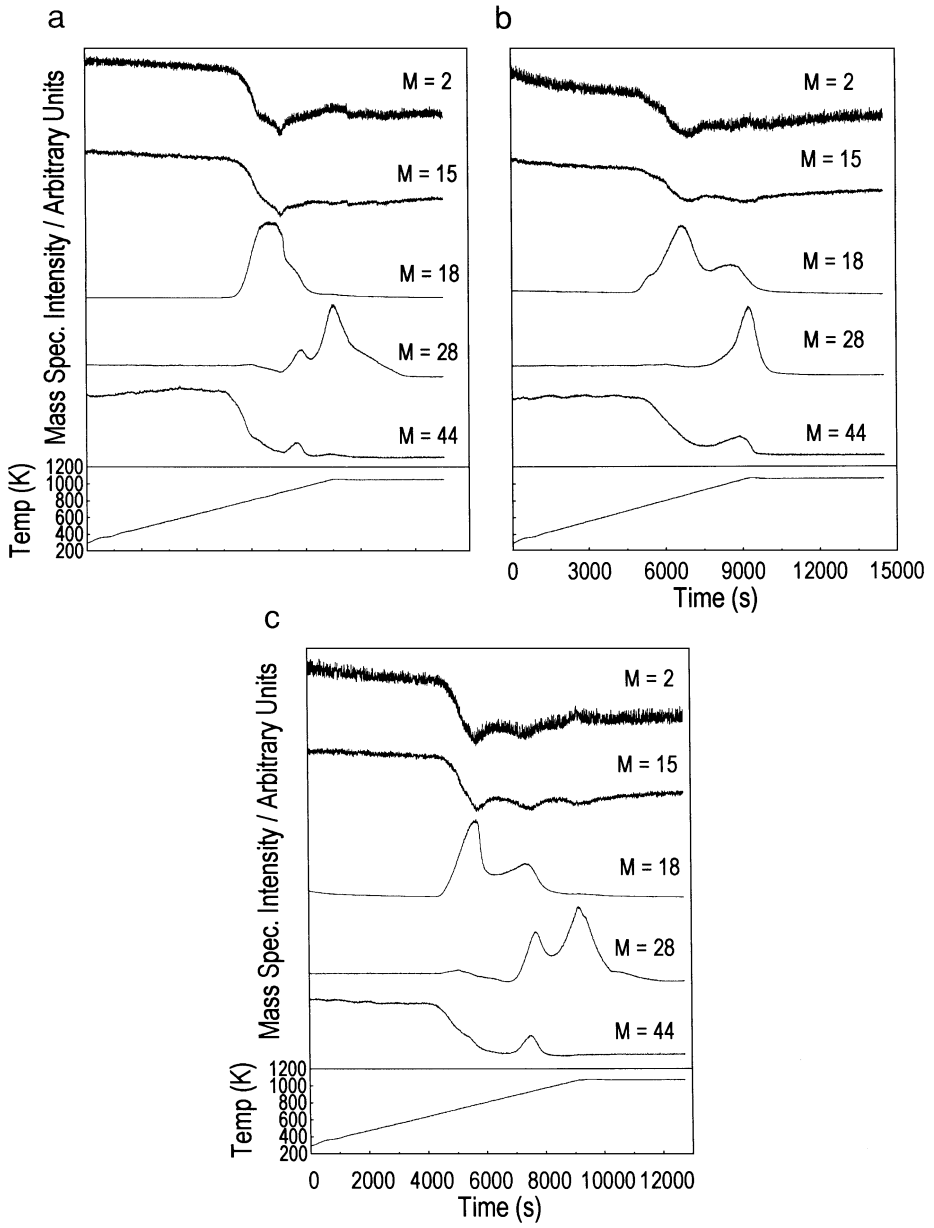

FIG. 3. Temperature programmed synthesis of bimetallic compounds. (a) V–Mo–O–C; (b) Nb–Mo–O–C; (c) Cr–Mo–O–C; (d) Fe–Mo–O–C; (e) Ni–Mo–O–C; (f) V–W–O–C; (g) Nb–W–O–C; (h) Mo–W–O–C; (i) Ni–W–O–C; (j) Fe–W–O–C; (k) Co–W–O–C.

TABLE 4

Characteristics of Bimetallic Oxycarbides

Sample	*In situ*			After passivation–reactivation		
	CO uptake (μmol g^{-1})	Surface area (S_g m^2 g^{-1})	Site density ($\times 10^{15}$ cm^{-2})	CO uptake (μmol g^{-1})	Surface area (S_g m^2 g^{-1})	Site density ($\times 10^{15}$ cm^{-2})
V–Mo–O–C	23	41	0.034	—	—	—
Nb–Mo–O–C	227	124	0.11	54	98	0.033
Cr–Mo–O–C	0	47	0	0	47	0
Fe–Mo–O–C	152	12	0.76	50	14	0.22
Ni–Mo–O–C	520	31	1.01	186	35	0.32
V–W–O–C	0	26	0	0	26	0
Nb–W–O–C	195	51	0.23	14	51	0.017
Mo–W–O–C	357	48	0.45	141	48	0.18
Ni–W–O–C	95	5.6	1.02	80	6.3	0.76
Co–W–O–C	0	7.9	0	0	8.7	0
Fe–W–O–C	0	5.2	0	0	5.4	0

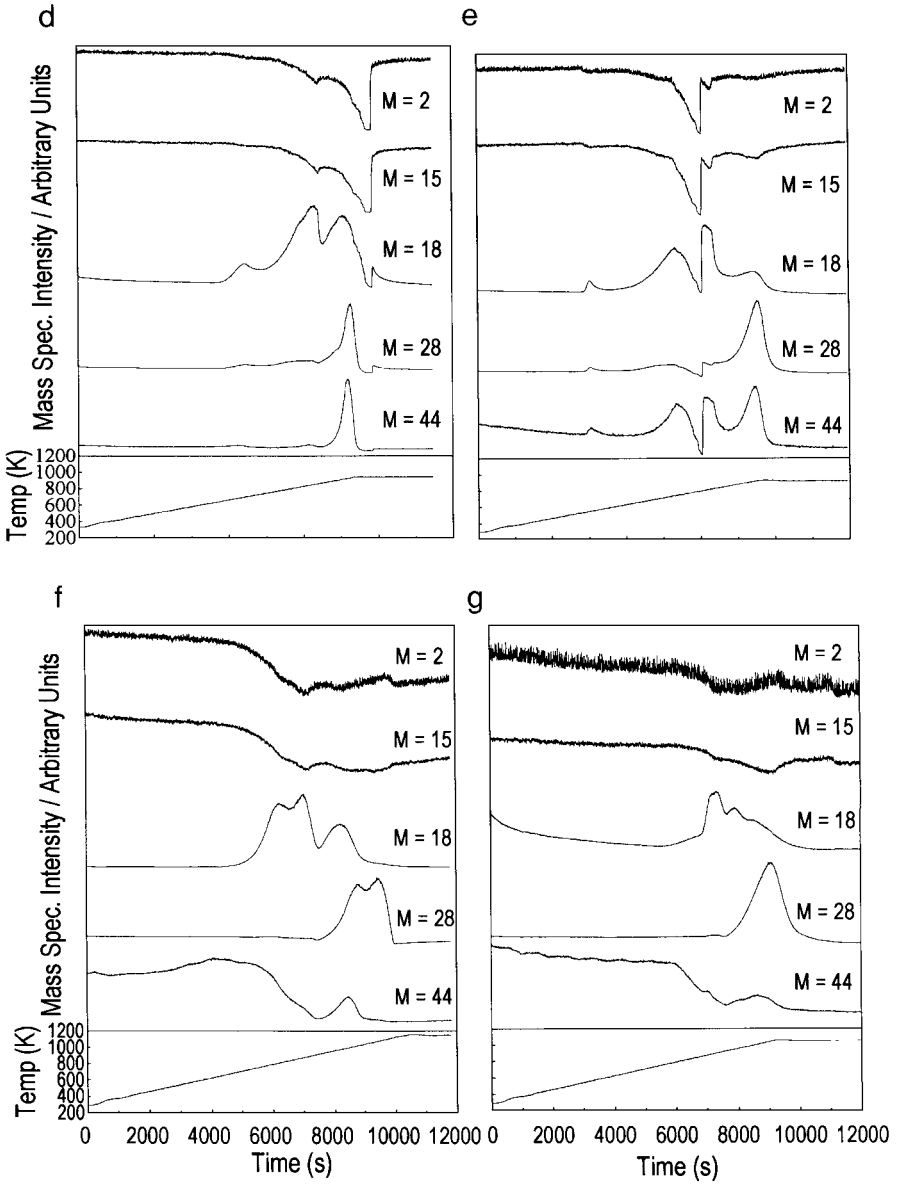

FIG. 3—*Continued*

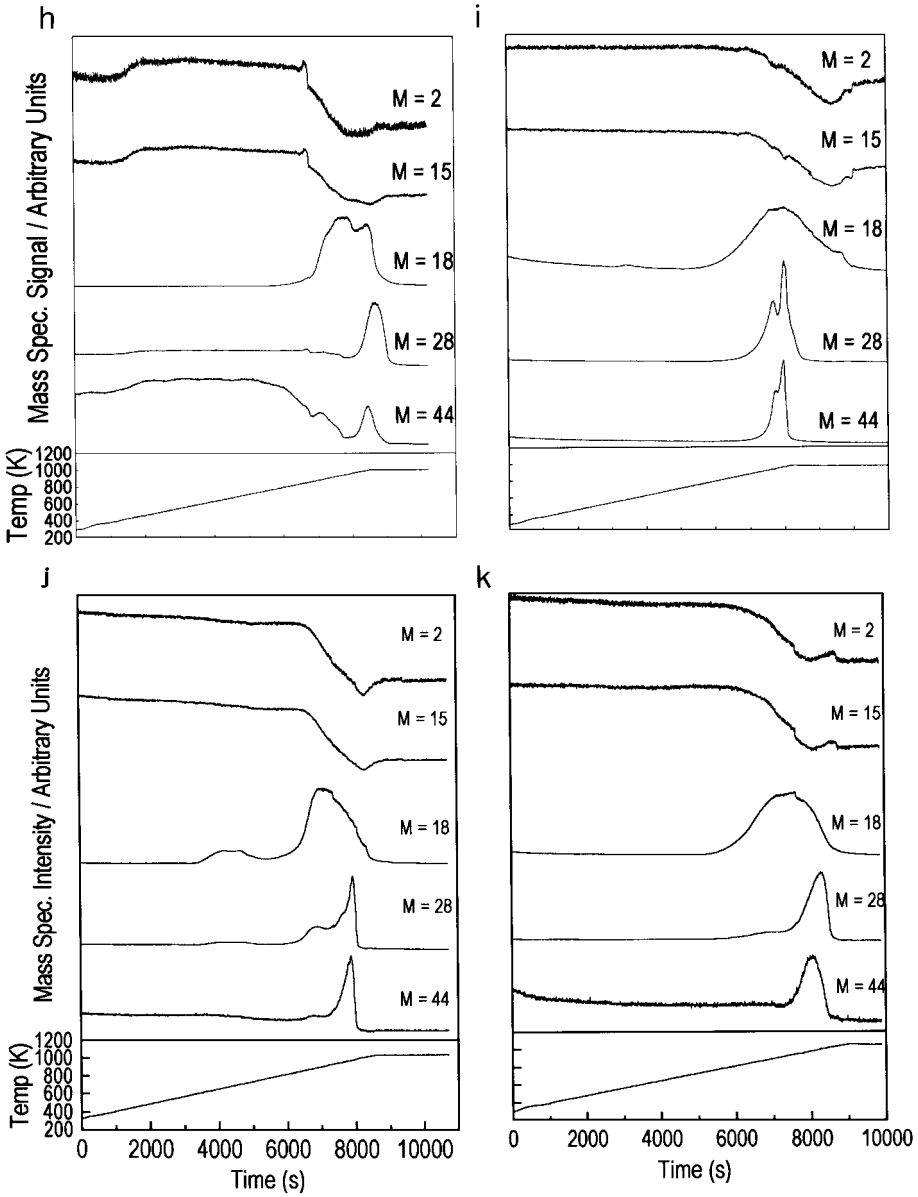

FIG. 3—*Continued*

Figures 5–7 show the temperature profiles as well as the TPR traces of samples after CO chemisorption then passivation. Masses at 2, 15, 18, 28, and 44 represent hydrogen, methane, water, carbon monoxide, and carbon dioxide, respectively.

Tables 5 and 6 summarize the results of the hydroprocessing activity studies. Tests are carried out on Nb–Mo–O–C, Mo–W–O–C, Ni–Mo–O–C, and Ni–W–O–C. A sulfided Ni–Mo–S/Al_2O_3 catalyst is used as a reference.

Figure 8 shows the XRD patterns of samples after reaction. They indicate that in some cases the catalysts are stable in the sulfur-containing stream, while in other cases they decompose into sulfides.

TABLE 5

Summary of Catalyst Performance in Hydroprocessing at 3.1 MPa and 643 K

Catalyst	% QNL Conversion HYD + HDN	HDN %	HDS %
Nb–Mo–O–C	86	44	57
Ni–Mo–O–C	70	20	40
Mo–W–O–C	65	10	3
Ni–W–O–C	50	0	20
Mo_2C*	86	58	45
WC*	81	28	16
NbC*	57	5	3
Ni–Mo–S/Al_2O_3	85	38	79

* Ref (35).

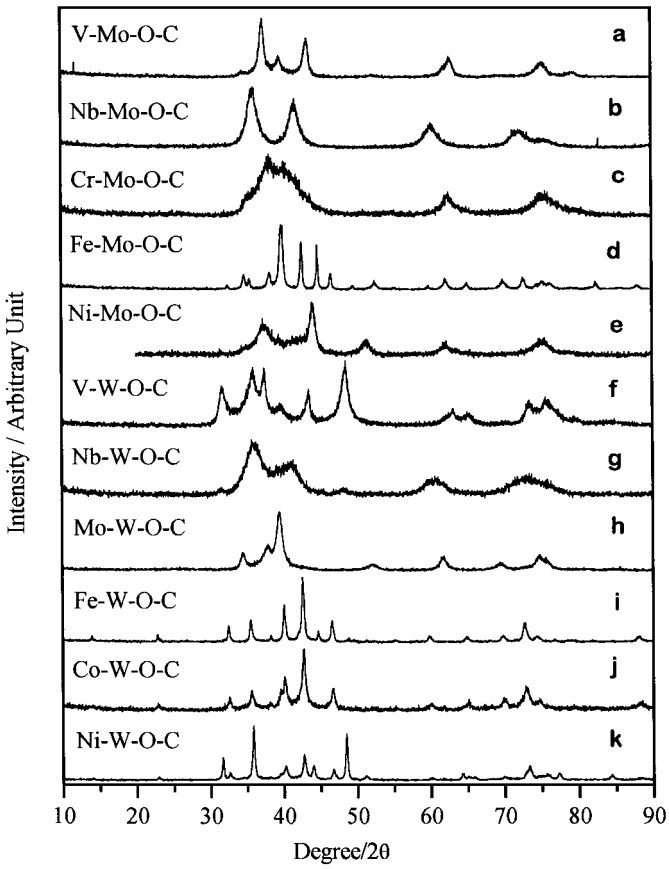

FIG. 4. X-ray diffraction patterns of bimetallic oxycarbides.

DISCUSSION

A. Synthesis

The preparation of the bimetallic carbides was carried out by the controlled carburization of bimetallic oxides. An important aspect of the synthesis was the use of true bimetallic precursors, for it is known that a physical mixture of oxides produces a mixture of carbides (33). For this reason considerable effort was expended on the preparation of ternary oxide compounds (Fig. 1) containing no traces of binary oxide components (Fig. 2). The preparation conditions for the mixed oxides (Table 1) were varied for each oxide compound to ensure complete solid state reaction of the constituents.

For the carburization, a temperature-programmed synthesis (TPS) method was employed which has been successful with single-metal carbides and nitrides (32, 34). The method consists of passing a carburizing gas mixture over the oxides while raising the temperature in a progressive manner to a final temperature, T_{max}. Importantly, the reactants (CH_4 and H_2) and principal products (CO, CO_2, H_2O) were followed in real time with a mass spectrometer to monitor the progress of the reaction. This allowed the temperature program to be stopped once the carburization reaction was finished, and thus, to avoid excessive heating of the samples. After reaching T_{max}, the samples were maintained at this temperature for a length of time, t_{hold}, to allow the reaction to go to completion. Obtaining the exact procedure for each sample required a number of trials and the final conditions are summarized in Table 2.

The temperature programmed synthesis traces (Fig. 3) show general features that are common to all compounds. The synthesis reaction always proceeds in two stages. First there is an initial reduction of the precursor oxide and then further reduction and carburization. Reduction is manifested as a decrease in the hydrogen mass spectrometer signal ($M = 2$) accompanied by simultaneous water ($M = 18$) evolution. Carburization is indicated by a decrease in the methane signal ($M = 15$) accompanied by peaks in the CO ($M = 28$), and sometimes CO_2 ($M = 44$), signals. Evidently, the methane also acts as a reducing agent. Because the CO signal was taken to be indicative of carburization, the maximum synthesis temperature (T_{max}) was chosen 5–20 K above the CO signal peak temperature.

As seen from the TPS traces each particular compound had its own response. For example, the initial water formation peak could appear alone or accompanied by higher temperature features. Similarly, the high temperature CO signal could be a single peak or a combination of peaks. An important generalization can be made, however. The samples can be divided into two groups: Group I includes Nb–Mo (Fig. 3b), Fe–Mo (Fig. 3d), Ni–Mo (Fig. 3e), Nb–W (Fig. 3g), Mo–W (Fig. 3h), Ni–W (Fig. 3i), while Group II includes V–Mo (Fig. 3a), Cr–Mo (Fig. 3c), V–W (Fig. 3f), Co–W (Fig. 3k), Fe–W (Fig. 3j). As will be seen, the compounds in Group I are easily reducible and have high CO chemisorption uptakes, while compounds in Group II are less reducible and have low uptakes. In terms of the TPS behavior, the compounds in Group I have a single high temperature CO peak, while those in Group II have two or more peaks. For Group I, the single CO peak is accompanied by a CO_2 feature of the same shape. However,

TABLE 6

Comparison of Turnover Rates of Bimetallic and Monometallic Carbides at 3.1 MPa and 643 K

Catalyst	Total turnover rate (s^{-1}) (HYD + HDN + HDS)	HDN turnover rate (s^{-1})
Nb–Mo–O–C	2.3×10^{-3}	1.3×10^{-3}
Ni–Mo–O–C	9.6×10^{-4}	2.0×10^{-4}
Mo–W–O–C	1.2×10^{-3}	1.8×10^{-4}
Ni–W–O–C	1.2×10^{-4}	—
Mo_2C[a]	3.0×10^{-3}	1.1×10^{-3}
WC[a]	3.7×10^{-3}	1.6×10^{-3}
NbC[a]	6.0×10^{-4}	4.9×10^{-4}
Ni-Mo-S/Al_2O_3	4.9×10^{-4}	6.5×10^{-4}

[a] Calculated based on the data reported in Ref. (35).

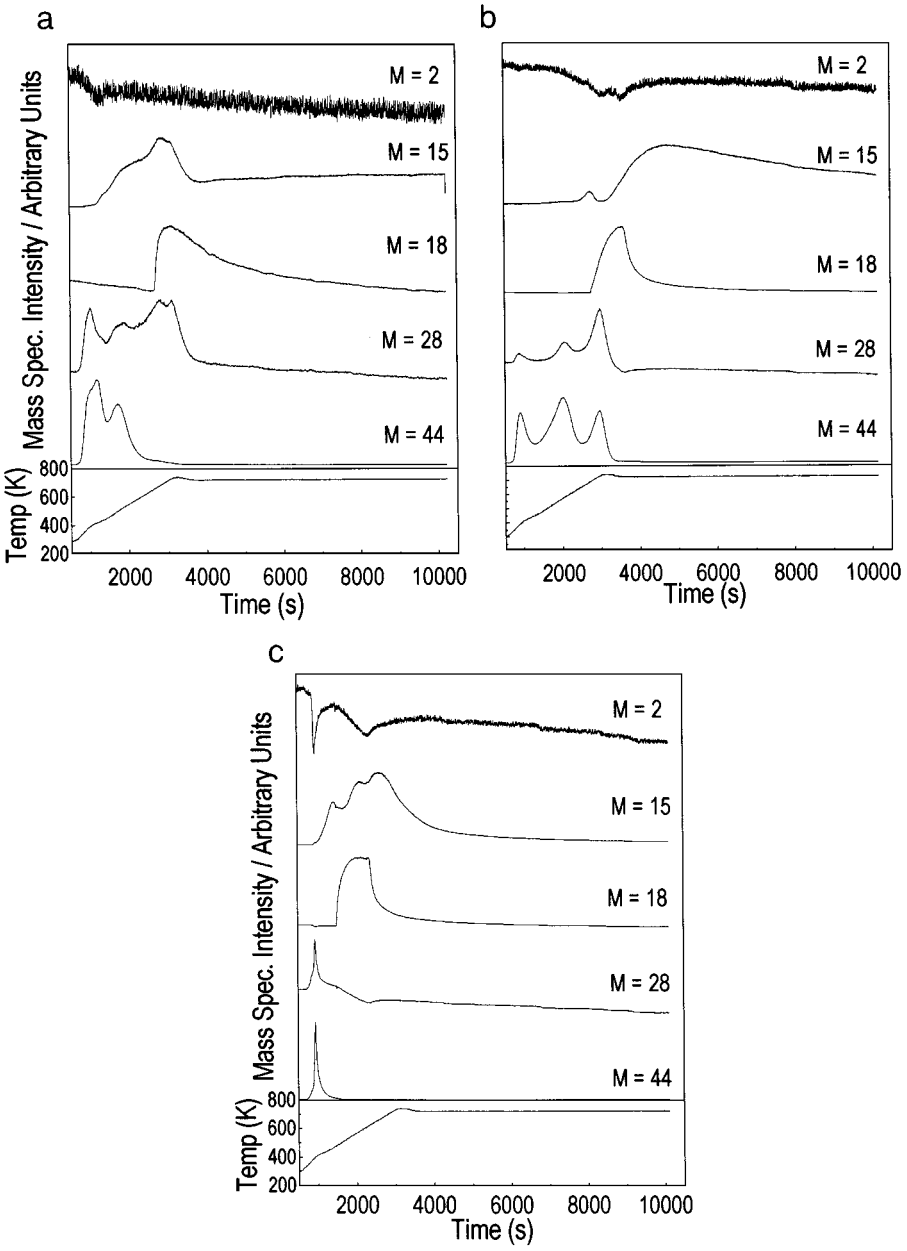

FIG. 5. Temperature programmed reduction of group I bimetallic oxycarbides. (a) Nb–Mo–O–C; (b) Fe–Mo–O–C; (c) Ni–Mo–O–C.

for Group II, generally only the low temperature CO peak has an associated CO_2 signal. Also, examination of Table 2 shows that the compounds of Group II generally require a higher synthesis temperature than those of Group I.

The reason for the presence of single versus multiple CO peaks is unclear. A single peak may be associated with the facile transformation of oxides to carbides with no intervening intermediate compounds as occurs in the topotactic transformation of MoO_3 to Mo_2N (35) or V_2O_5 to VN (36). The ease of replacement of oxygen by nitrogen or carbon in such reactions is due to high atomic mobility and may explain the relative reducibility of these compounds.

There are other connections between composition and synthesis temperature. The molybdenum compounds in general have lower transformation temperatures than the tungsten compounds, but there are exceptions (e.g., Nb–Mo > Nb–W). Also, compounds with the late transition metals (Fe, Co, Ni) tend to have lower reaction temperatures than those with the early transition metals (V, Nb, Cr).

There was a considerable amount of water formation during the initial reduction. The leak valve suffered a decrease in gas conduction because of condensation. This is seen in a shift in the base line for the hydrogen ($M = 2$) and methane

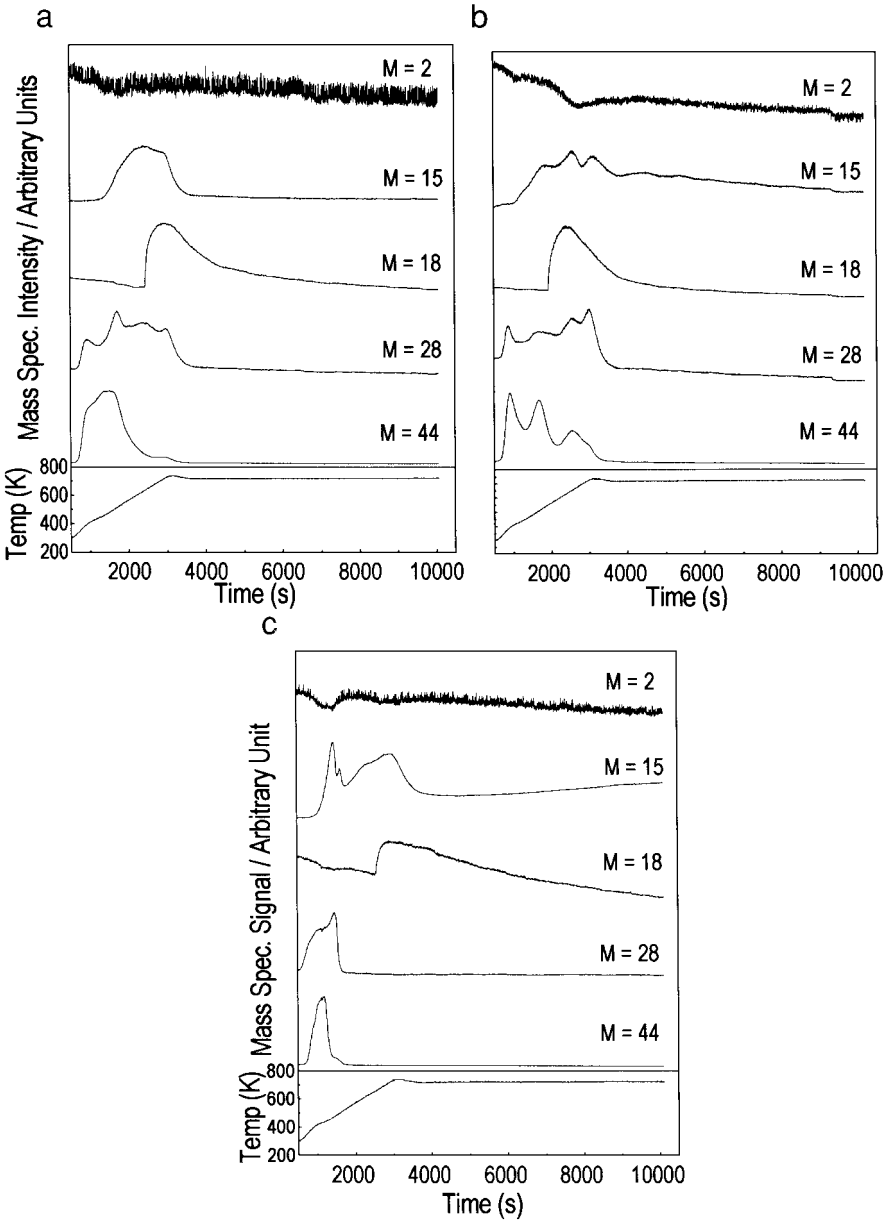

FIG. 6. Temperature programmed reduction of group I bimetallic oxycarbides. (a) Nb–W–O–C; (b) Mo–W–O–C; (c) Ni–W–O–C.

($M = 15$), and carbon dioxide ($M = 44$) signals. In two cases, actual clogging caused discontinuities in the reaction traces (Fe–Mo–O–C and Ni–Mo–O–C, Figs. 3d and 3e). Since this occurred in the exit lines, there was no effect on the actual synthesis of the compounds.

B. Characterization

The elemental composition of a number of the compounds is reported in Table 3. For the metals, there is good agreement between the measured compositions and the theoretically expected compositions from the synthesis conditions. The slight deviations are consistent with evaporation of the more volatile oxide during the calcination step for the preparation of the mixed oxide. A notable feature of the present compounds is the high proportion of the nonmetal atoms, C and O. This is due to two factors. The first is that nonstoichiometry is very common in carbides and nitrides, with deviations occurring both in metal and in nonmetal (37, 38). In this case, there is formation of metal vacancies, a reasonable result since the starting materials were oxides not metals. The second factor is the relatively high surface area of the materials which results in a substantial contribution of the passivation layer on the oxygen content. This has been estimated to be up to 25 mol% of the oxygen in the sample (1).

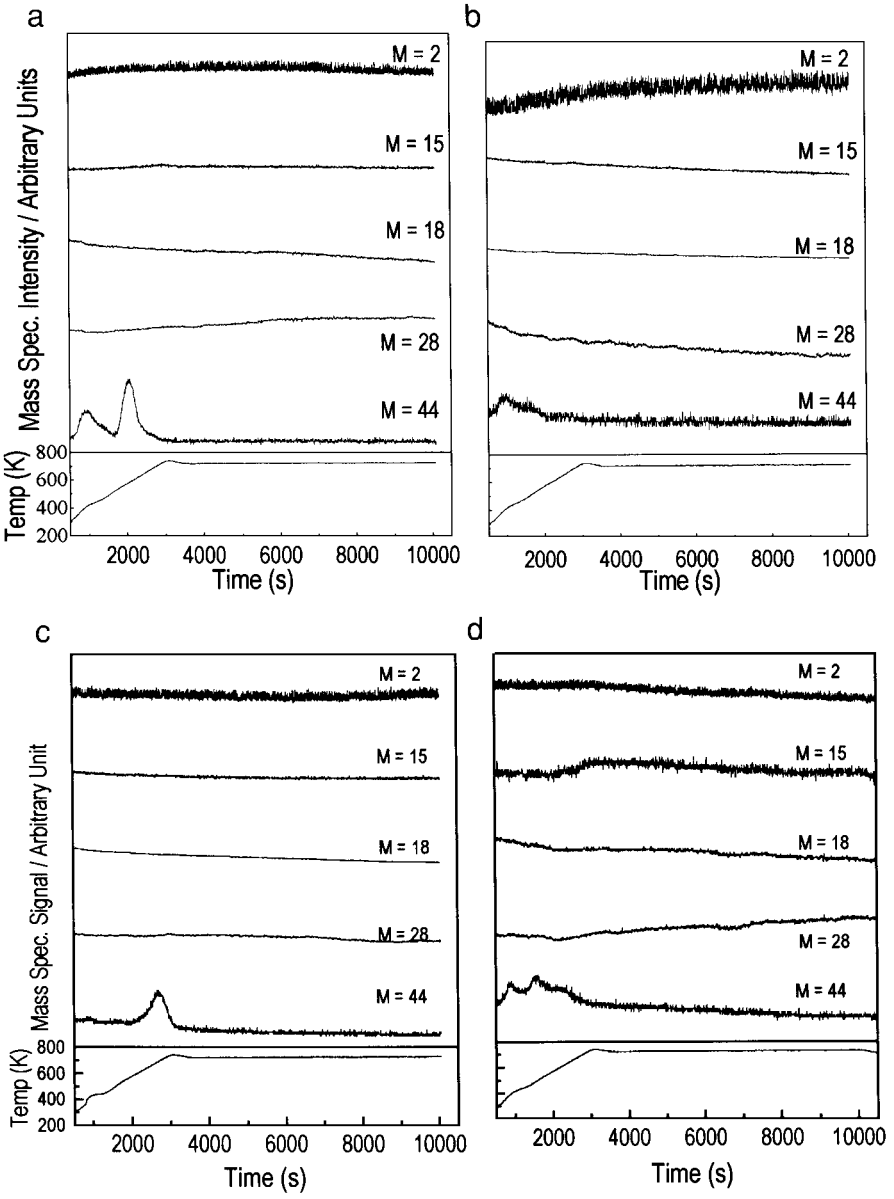

FIG. 7. Temperature progrmmed reduction of group II bimetallic oxycarbides. (a) Cr–Mo–O–C; (b) V–W–O–C; (c) Co–W–O–C; (d) Fe–W–O–C.

The crystal structure of the materials was determined by powder X-ray diffraction. Unlike the analogous bimetallic transition metal oxynitrides (1), which have a simple B1 cubic (NaCl type) structure (space group $Fm3m$), the bimetallic oxycarbides adopt various kinds of structure. Nb–Mo–O–C has a simple B1 cubic ($Fm3m$) structure, Mo–W–O–C has a hexagonal closed pack ($P63/mmc$) structure. Both Fe–W–O–C and Co–W–O–C have a cubic η-carbide phase with Fe_3W_3C type structure ($Fd3m$). The XRD results indicate that both Cr–Mo–O–C and Nb–W–O–C have low crystallinity; however, their XRD patterns still suggest the materials have cubic ($Fm3m$) structure.

In some cases, phase separation occurs during the temperature programmed reaction, and the final products consist of mixed phases. V–Mo–O–C is a two-phase mixture, the major phase has a B1 cubic ($Fm3m$) structure, and the minor phase has a hexagonal structure ($P63/mmc$). Fe–Mo–O–C also contains mixed phases: the major phase has a hexagonal structure ($P63mc$), one of the minor phases has a hexagonal closed packed structure ($P63/mmc$), and the other minor phase has a cubic ($Fd3m$) symmetry. The two phases in V–W–O–C can be indexed to a WC-type simple hexagonal structure and a B1 cubic structure ($Fm3m$). The major phase in Ni–W–O–C has a WC-type simple hexagonal structure, the two minor phases have cubic symmetry ($Fd3m$ and $Fm3m$). The Ni–Mo–O–C has an unusual pattern that could be due to a mixture of hexagonal ($P63mc$) and cubic ($Fm3m$) structures.

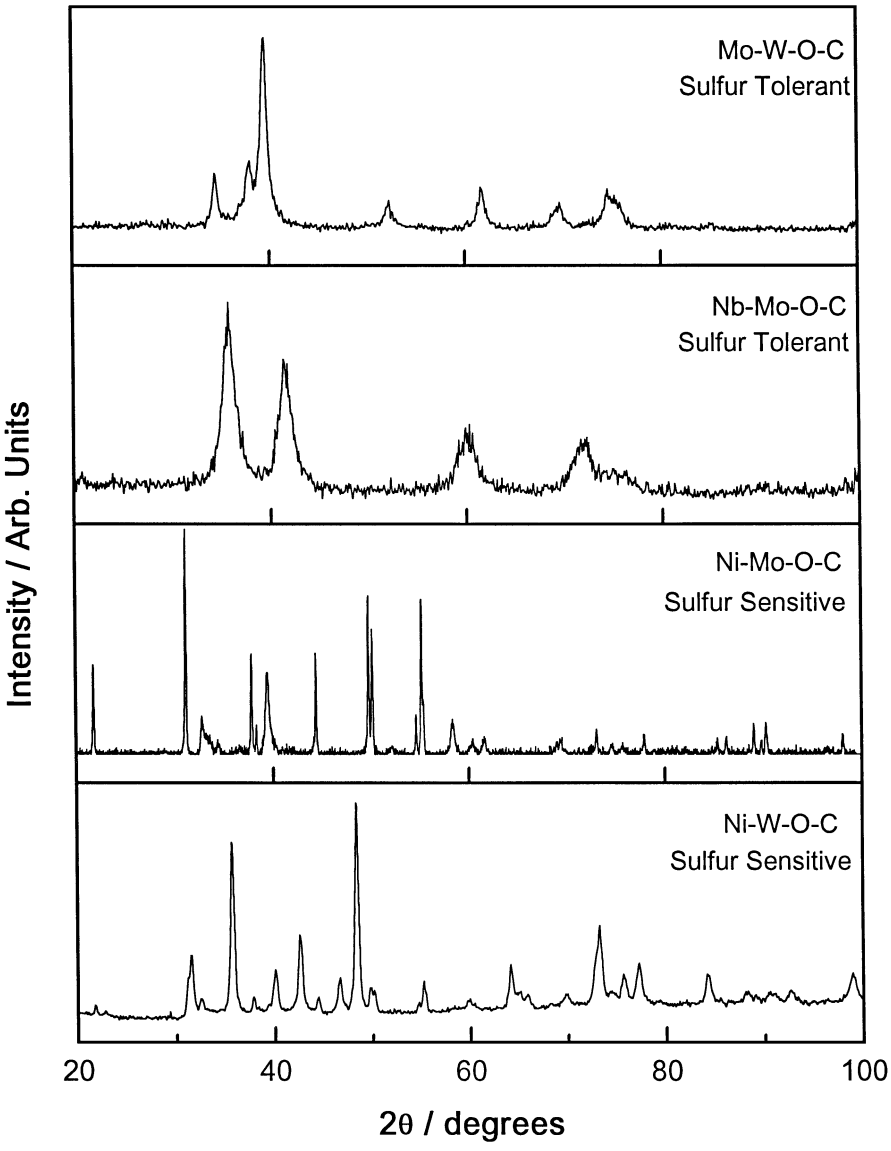

FIG. 8. X-ray diffraction patterns of bimetallic oxycarbides after reaction.

There is no strong connection between composition and phase purity. The early transition metals tend to form single-phase compounds of cubic or hexagonal structure (Nb–Mo, Nb–W, Mo–W, Cr–Mo). The exception is V which forms a mixture of cubic and hexagonal phases, possibly because of the similarity in stability of these two phases. The late transition metals tend to form pure η-carbide phases with W (Co–W, Fe–W), but with Mo (Fe–Mo, Ni–Mo) mixtures of cubic and hegagonal phases are formed.

The surface areas and CO uptakes of the samples are reported in Table 4. The surface areas range from low values ($\sim$5 $m^2 g^{-1}$) for the Fe–W, Co–W, and Ni–W compounds to a high value (120 $m^2 g^{-1}$) for the Nb–Mo compound. The chemisorption of CO can be used to titrate accessible surface metal atoms in these materials (39, 40). The measurements in this study were carried out at two conditions: on the freshly prepared samples not exposed to the atmosphere (refered to as *in situ* samples) and on passivated and rereduced samples.

The compounds can be divided according to the quantity of CO uptake into the two groups mentioned in the preparation section. For the Group I samples (Nb–Mo, Fe–Mo, Ni–Mo, Nb–W, Mo–W, Ni–W) the uptakes of CO range from moderate to high, while for the Group II compounds (V–Mo, Cr–Mo, V–W, Co–W, and Fe–W) the uptakes are low. It is not clear why chemisorption was low for the Group II compounds. As was noted earlier these materials required among the highest synthesis temperatures, and it may be that at these high temperatures excessive pyrolytic carbon was deposited on their surfaces.

The ratio of the CO uptake to the surface area gives the metal site density, which for a clean surface for these materials is on the order of 1×10^{15} cm^{-2}. For the Group I samples the values ranged from 0.11×10^{15} to 1.0×10^{15}. The two Ni compounds (Ni–Mo, Ni–W) showed the highest values, indicating that their surfaces were essentially clean. This could be a result of the reducing properties of Ni.

Although the surface area of samples after the passivation–reactivation basically remains unchanged, the CO uptakes decrease dramatically (Table 4). Compared with the freshly prepared *in situ* value, the CO uptakes of most reactivated samples show more than a 150% decrease. The only exception is Ni–W–O–C, which has a minor 18% decrease. The reduction in the CO uptake is likely due to the retention of strongly chemisorbed oxygen on the passivated samples. In order to better understand the situation, TPR studies in hydrogen were carried out on the samples. Importantly, the final temperature was set at 723 K (450°C), the temperature of activation of the compounds prior to both chemisorption and catalytic testing. XRD indicated that the samples were stable to reduction at these conditions.

The evolving gases during the temperature-programmed reduction to 723 K in 10% H_2/He include CO, CO_2, H_2O, and CH_4. The appearance of CO_2 indicates strong interaction between surface carbon and oxygen. In many cases the CO and CO_2 traces show quite complicated multipeak patterns, which suggests the presence of different types of bonding in the oxycarbides.

According to the TPR traces, the oxycarbides can be again categorized into the same two groups as before. Group I has relatively high chemisorption uptakes and strong TPR desorption signals (Figs. 5 and 6). This first group includes Ni–Mo–O–C (Fig. 5c) and Ni–W–O–C (Fig. 6c), the two compounds with the highest site density. The TPR traces show relatively simple but high intensity CO and CO_2 patterns, as well as substantial methane formation. Thus, some decarburization occurred during the pretreatment. Group I also includes Mo–W–O–C, Fe–Mo–O–C, Nb–Mo–O–C, and Nb–W–O–C with medium site density. In terms of TPR traces, the intensity of CO, CO_2, and CH_4 signals are moderate, and the peak shape of CO and CO_2 traces are quite complex. Group II includes Cr–Mo–O–C, V–W–O–C, Co–W–O–C, Fe–W–O–C, and Nb–W–O–C (Fig. 7). Their TPR traces show few desorption traces, except for some CO_2 formation, suggesting very low surface activity. In fact, these compounds do not have significant CO uptake.

C. Reactivity

The activities of the bimetallic carbides and the commercial Ni–Mo–S catalyst were compared on an equal reactor loaded surface area of 30 m^2. Only four bimetallic carbides of Group I were studied, because they had high values of CO uptake and moderate surface areas: Nb–Mo, Ni–Mo, Mo–W, and Ni–W. Table 5 presents the steady state HYD, HDN, and HDS activities of the catalysts. The products identified from quinoline HDN were hydrogenated quinoline compounds and denitrogenated hydrocarbons. The major hydrogenated (HYD) quinoline compounds identified were 1,2,3,4 tetrahydroquinoline (1-THQ) and 5,6,7,8 tetrahydroquinoline (5-THQ), while decahydroquinoline (DHQ) was detected in small amounts. The major hydrodenitrogenated (HDN) hydrocarbons were propylcyclohexane (PCH) and propylbenzene (PBZ). Small amounts of benzene and cyclohexane were also detected. The steady state HDN conversions of the catalysts ranged from 0–44%, with Nb–Mo–O–C showing the highest HDN activity (44%) followed by Ni–Mo (20%), Mo–W (10%), and Ni–W (0%). The exclusive product of dibenzothiophene HDS was biphenyl.

The product distribution is consistent with a denitrogenation network (32) proceeding through the hydrogenation of both aromatic rings of quinoline and then a rapid hydrogenolysis of DHQ to yield propylcyclohexane or a reactive intermediate, propylcyclohexene (PCHE). Since PCHE is a very reactive compound, it is expected to undergo ready hydrogenation to PCH or dehydrogenation to PBZ. This also explains the formation of PBZ in the absence of o-propylaniline (OPA) in the products.

The steady state HDS activity of the bimetallic carbides ranged from 0–57%, with the Nb–Mo–O–C catalyst exhibiting the highest HDS conversion (57%), followed by Ni–Mo (40%) and Ni–W (20%). The moderate HDS activity of Ni-containing bimetallic catalysts could be due to the propensity of Ni to form a sulfide phase, which is known to exhibit HDS activity. On the other hand, the sulfur tolerant bimetallic carbides seem to exhibit lower HDS activity, which was also observed for the monometallic carbide catalysts (Mo_2C, WC).

The Nb–Mo–O–C had better HDN activity than the sulfided Ni–Mo–S/Al_2O_3 catalyst on an equal surface area basis. Comparison of activity between unsupported and supported samples needs to be done carefully. In this case, though, the sulfide is a high loading (>20 wt%) commercial sample and should be highly optimized so that most of its surface should be active. This was confirmed by measurements of O_2 chemisorption at low temperatures (dry-ice/acetone) which indicated high dispersion of the sulfide phase. On a volume basis the supported catalyst is superior; however, what is important from a fundamental standpoint is an areal comparison which is a better measure of the intrinsic activity. The bimetallic compounds could be deposited on a support to improve their volumetric activity.

The Nb–Mo–O–C sample was studied in depth because of its high activity (4). Near edge X-ray absorption fine structure (NEXAFS) measurements taken in the electron yield mode (surface sensitive) indicated the formation of a true

bimetallic compound. X-ray photoelectron spectroscopy (XPS) analysis before reaction confirmed the presence of an oxycarbide surface. After reaction, the surface remained an oxycarbide with only 2 mol% sulfur in the near-surface region. For molybdenum nitride used for hydrotreating a vacuum gas oil (41), it was found that a surface sulfide was formed. However, in that study the sulfur content of the feed was 30,000 ppm (3%), in contrast to the 3000 ppm used in the present work. This does not rule out the formation of a special sulfur-containing phase, perhaps a carbosulfide, on the surface of these materials (42). On bimetallic nitrides enhanced HDS activity over monometallic nitrides in hydroprocessing has been reported, and this has been attributed to the formation of increased sites (20) or the exposure of (111) planes (21, 22).

Figure 8 presents the XRD patterns of the spent catalysts. Extraneous oxide or sulfide phases were not observed in the catalysts involving Mo, W, and Nb indicating that these catalysts were tolerant of sulfur at the reaction conditions. However, sulfide peaks were observed in the XRD patterns of the catalysts involving Ni. The spent Ni–Mo–O–C catalyst does not show any features of the fresh catalyst indicating a complete change in the bulk composition after exposure to the reaction conditions. The peaks in the XRD pattern can all be assigned to Ni_3S_2 (PDF file 30-863) and MoS_2 (PDF file 37-1492). The spent Ni–W–O–C retains the essential features of the original structure, but additional XRD peaks can be assigned to Ni_3S_2 and WS_2 (PDF file 35-651).

The total activity (HYD, HDN, and HDS) and the HDN activity are reported in the form of turnover rates based on CO chemisorption for the bimetallic carbides in Table 6. The general trends in conversion (Table 5) are paralled in these rates. For the most part the bimetallic compounds have activity close to that of the monometallic compounds. In particular, the bimetallic carbide, Nb–Mo–O–C, has a total rate comparable to that of Mo_2C, the most active of the monometallic carbides (32). This result is reproducible and can be improved with variation of the composition (4). Thus, bimetallic systems offer the possibility of further enhancements in carbide performance. This could be achieved by optimization of the composition, the use of supports, or the addition of promotors.

CONCLUSIONS

1. A series of materials consisting of bimetallic oxycarbides of Mo and W in combination with transition metals of groups 5–10 were prepared.

2. The structure of the compounds ranges from cubic to hexagonal structures for the early transition metals and κ- or η-structures for the late transition metals.

3. The compounds can be divided into two groups, with different synthesis, chemisorption, and reduction properties.

4. The compounds have moderate activity in hydroprocessing with most resembling the monometallic carbides.

ACKNOWLEDGMENTS

We thank Dr. Fawzy Sherif for help with the elemental analysis. Funding for this work from the Department of Energy, Office of Basic Energy Sciences, Grand DE-FG02-96ER14669, the DOE Advanced Coal Research at U.S. Universities Program, Grant DE-FG26-97FT97265, and Akzo Nobel is greatly appreciated.

REFERENCES

1. Yu, C. C., Ramanathan, S., and Oyama, S. T., *J. Catal.* **173**, 1 (1998).
2. Ramanathan, S., Yu, C. C., and Oyama, S. T., *J. Catal.* **173**, 10 (1998).
3. Kapoor, R., Oyama, S. T., Frühberger, B., and Chen, J. G., *J. Phys. Chem. B* **101**, 1543 (1997).
4. Yu, C. C., Ramathan, S., Dhandapani, B., Chen, J. G., and Oyama, S. T., *J. Phys. Chem. B* **101**, 512 (1997).
5. Oyama, S. T., "The Chemistry of Transition Metal Carbides and Nitrides," Blackie Academic and Professional, London, 1996.
6. Kojima, I., Miyazaki, E., and Yasumori, I., *J. Chem. Soc. Comm.* 573 (1980).
7. Kojima, I., Miyazaki, E., Inoue, Y., and Yasumori, I., *J. Catal.* **73**, 128 (1982).
8. Kojima, I., and Miyazaki, E., *J. Catal.* **89**, 168 (1984).
9. Oyama, S. T., Schlatter, J. C., Metcalfe, J. E., III, and Lambert, J. M., Jr., *Ind. Eng. Chem. Res.* **27**, 1639 (1988).
10. Schlatter, J. C., Oyama, S. T., Metcalfe, J. E., III, and Lambert, J. M., Jr., *Ind. Eng. Chem. Res.* **27**, 1648 (1988).
11. Leclerco, L., Provost, M., Pastro, H., and Grimblot, J., *J. Catal.* **117**, 371 (1989).
12. Levy, R. B., and Boudart, M., *Science* **181**, 547 (1973).
13. Colton, R. J., Huang, J. J., and Rabalais, J. W., *Chem. Phys. Lett.* **34**, 337 (1975).
14. Lee, J. S., Oyama, S. T., and Boudart, M., *J. Catal.* **106**, 125 (1987).
15. Ranhotra, G. S., Bell, A. T., and Reimer, J. A., *J. Catal.* **108**, 40 (1987).
16. McCrea, K., Logan, J. W., Tarbuck, T. L., Heiser, J. L., and Bussell, M. E., *J. Catal.* **171**, 255 (1997).
17. Dolce, G. M., Savage, P. E., and Thompson, L. T., *Energy Fuels* **11**, 668 (1997).
18. Nagai, M., Irisawa, A., and Omi, S., *J. Phys. Chem. B* **102**, 7619 (1998).
19. Ozkan, U., Zhang, L., and Clark, P. A., *J. Catal.* **172**, 294 (1997).
20. Logan, J. W., Heiser, J. L., McCrea, K. R., Gates, B. D., and Bussell, M. E., *Catal. Lett.* **56**, 165 (1998).
21. Li, Y., Zhang, Y., Raval, R., Li, C., Zhai, R., and Xin, Q., *Catal. Lett.* **48**, 239 (1997).
22. Zhang, Y., Li, Y., Raval, R., Li, C., Zhai, R., and Xin, Q., *J. Molec. Catal.* **132**, 241 (1998).
23. Hägg, G., *Z. Phys. Chem.*, Abt. **B12**, 33 (1931).
24. Oyama, S. T., *J. Solid State Chem.* **96**, 442 (1992).
25. Nowotny, H., and Benesovsky, F., *in* "Phase Stability in Metals and Alloys" (P. S. Rudman, J. Stringer, and R. I. Jaffee, Eds.), p. 329. McGraw-Hill, New York, 1967.
26. Jeitschko, W., Nowotny, H., and Benesovsky, F., *Monatsh. Chem.* **94**, 247 (1963).
27. Huetter, L. J., and Stadelmaier, H. H., *Acta Met.* **6**, 367 (1958).
28. Jeitschko, W., Nowotny, H., and Benesovsky, F., *Monatsh. Chem.* **94**, 672 (1963).
29. Schönberg, N., *Acta Met.* **2**, 837 (1954).

30. Chianelli, R. R., Jacobson, A. J., Kugler, E. L., and McCandlish, L. E., European Patent Application: 89305198.7 (1989).
31. Rautala, P., and Norton, J. T., *J. Met.* **5**, 745 (1953).
32. Ramanathan, S., and Oyama, S. T., *J. Phys. Chem*. **99**, 16365 (1995).
33. Teixeira, V. L. S., Schmal, M., Schwartz, M., and Oyama, S. T., *J. Mater. Res.* **13**, 1977 (1998).
34. Volpe, L., and Boudart, M., *J. Solid State Chem*. **59**, 348 (1985).
35. Volpe, L., and Boudart, M., *J. Solid State Chem*. **59**, 332 (1985).
36. Kapoor, R., and Oyama, S. T., *J. Solid State Chem*. **99**, 303 (1992).
37. Juza, R., and Sachsze, S., *Z. Anorg. Chem*. **253**, 95 (1945).
38. Juza, R., *in* "Advances in Inorganic Chemistry and Radiochemistry" (H. J. Emeleus and A. G. Sharpe, Eds.), Vol. 9, p. 81. Academic Press, New York and London, 1966.
39. Lee, J. S., Lee, K. H., and Lee, J. Y., *J. Phys. Chem*. **96**, 362 (1992).
40. Lee, J. S., Locatelli, S., Oyama, S. T., and Boudart, M., *J. Catal.* **125**, 157 (1990).
41. van Veen, J. A. R., Minderhoud, J. K., Buglass, J. G., Lednor, P. W., and Thompson, L. T., *Mat. Res. Soc. Symp. Proc.* **368**, 51 (1995).
42. Dhandapani, B., St. Clair, T., and Oyama, S. T., *Appl. Catal. A Gen* **168**, 219 (1998).